DNS of helical vortices

Ivan Delbende(1,2), **Maurice Rossi**(1,3), **Benjamin Piton**(1,2)

(1) *UPMC, Université Pierre et Marie Curie-Paris 6, France*
(2) *LIMSI–CNRS, UPR3251, BP133, 91403 Orsay Cedex, France*
Email : Ivan.Delbende@limsi.fr, Benjamin.Piton@limsi.fr
(3) *IJLRA–UPMC, UMR7190, 75232 Paris Cedex 05, France*
Email : Maurice.Rossi@upmc.fr

1 Introduction

Rotating devices such as propellers, wind turbines, helicopter rotors are known to develop a system of helical vortices in their wake. These structures result from the rapid roll-up of the vorticity sheet continuously generated at the trailing edge of the rotating blades. Experiments show that they interact with the mean flow : the radius of helical tip vortices follows the expansion (resp. the contraction) of the fluid tube passing through the turbine (resp. the propeller) and becomes constant within a downstream distance comparable to the diameter of the rotating device. At this distance, the fluid system — apart from turbulent fluctuations — has locally become helically symmetrical, meaning that it is locally invariant through combined axial translation and rotation about the same axis. In most real situations, this property does not hold into the far wake : instabilities often develop and drive the system to a fully three-dimensional turbulent flow. In some cases, a bifurcation may lead to a completely different wake structure, as in the case of the vortex ring state in helicopter flight [1]. In all instances however, it is of great interest to have a reliable description of the reference helical flow at sufficiently high Reynolds number, so that its subsequent evolution can be predicted, for instance, by standard instability theory.

Earlier descriptions of such helical vortex systems made use of the vortex-filament model. On one hand, Hardin [2] gives an expression for the velocity field induced by a helical vortex filament on the surrounding fluid. This is useful to compute the angular velocity induced by this vortex onto another vortex of the wake (mutual induction). On the other hand, it is also necessary to evaluate the velocity induced by the vortex filament on itself (self-induction). This can be done either by the cutoff theory whereby the singularity of the filamentary Biot–Savart law is removed [3, 4] or by analytical developments on Hardin's solution [5]. Further extensions to helical vortex tubes with finite core size have also been developed [6]. All these studies are aimed at analytically predict the motion of a helical vortex system with prescribed geometry (helix radius, helix pitch and, when necessary, vorticity distribution within the core).

In the small core limit and in the inviscid framework, such solutions are known to be "shape-preserving" meaning that they are stationnary in a reference frame rotating at the angular velocity predicted for the system. When the core size is finite, the question is raised whether a given vorticity distribution may yield a stationary state or not. In a numerical study, Lucas & Dritschel [7] recently answered this question for the particular case of inviscid helical vortex patches (uniform vorticity within the core) with prescribed helix radius and vortex core size. Note that the above studies are all strictly restricted to the inviscid framework, a condition for the existence of stationary motion without any forcing.

As mentionned before, wake vortices form through the roll-up of the trailing vorticity sheet, and viscous diffusion eventually leads to continuous distributed vorticity distributions within the vortex cores, such as Gaussian. Moreover, a distribution of axial velocity may also be present, which has always been disregarded in the literature. The complexity of this general problem would lead to use a three-dimensional DNS code. However, the attainable Reynolds numbers are still moderate and long-time dynamics clearly out of reach with nowadays facilities. We present here an original numerical code aimed at describing the viscous dynamics of helical vortex systems, and more generally helically symmetrical flows by direct numerical simulation of the incompressible Navier–Stokes equations. The enforcement of the helical symmetry allows one to reduce the three-dimensional equations to a modified two-dimensional unsteady problem. The code thus takes into account 3D vortex curvature and torsion effects through the helical symmetry, but the resolution is of a 2D type, allowing for larger numbers of grid points and Reynolds numbers.

The Navier–Stokes equations with helical symmetry are presented in section §2. The numerical formulation is described in section §3. Viscous quasi-steady states consisting in one or several helical vortices are presented in section §4. Long-time (or equivalently far-wake) dynamics have also been investigated and different types of merging of helical vortices are presented in section §5. Concluding remaks are given in section §6.

2 Navier–Stokes equations with helical symmetry

A flow displays *helical symmetry* of *helix pitch* $2\pi L$ along a given axis when its velocity field is unaffected by an axial translation given by a length parameter Δz followed by a rotation of angle $\Delta\theta = \Delta z/L$ around the same axis as depicted in figure 1. The flow characteristics remain invariant along the helical lines $\theta - z/L =$ const. $L > 0$ corresponds to a right-handed helix and $L < 0$ to a left-handed helix.

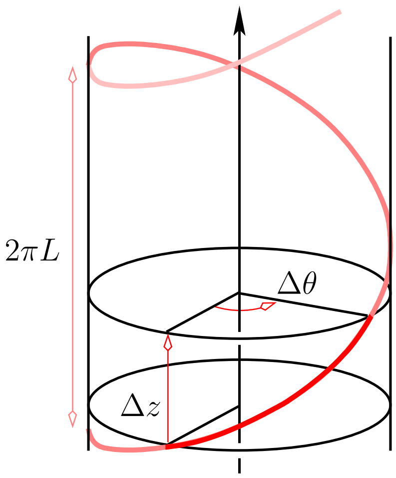

FIGURE 1 – *Right-handed helix of reduced pitch* L.

A scalar field f possesses helical symmetry if it depends only on the two space variables r and $\varphi \equiv \theta - z/L$ instead of the three coordinates r, θ and z. For a vector field $\boldsymbol{u}$, helical symmetry means that it can be written as

$$\begin{aligned}\boldsymbol{u} &= u_r(r,\varphi,t)\boldsymbol{e}_r(\theta)\\ &+ u_\varphi(r,\varphi,t)\boldsymbol{e}_\varphi(r,\theta)\\ &+ u_B(r,\varphi,t)\boldsymbol{e}_B(r,\theta)\end{aligned} \qquad (1)$$

where the orthogonal Beltrami basis $(\boldsymbol{e}_r, \boldsymbol{e}_\varphi, \boldsymbol{e}_B)$, presented in figure 2, is such that

$$\begin{aligned}\boldsymbol{e}_B(r,\theta) &= \alpha(r)\left[\boldsymbol{e}_z + \frac{r}{L}\boldsymbol{e}_\theta(\theta)\right],\\ \boldsymbol{e}_\varphi(r,\theta) &= \boldsymbol{e}_B \times \boldsymbol{e}_r = \alpha(r)\left[\boldsymbol{e}_\theta(\theta) - \frac{r}{L}\boldsymbol{e}_z\right]\end{aligned} \qquad (2)$$

with quantity $\alpha(r)$ defined as

$$\alpha(r) = \left(1 + \frac{r^2}{L^2}\right)^{-\frac{1}{2}}, \quad 0 \le \alpha(r) \le 1\,. \qquad (3)$$

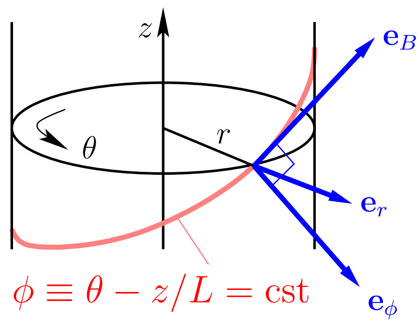

FIGURE 2 – *Local helical basis.*

A general incompressible helical flow can be expressed with only two scalar fields as :

$$\boldsymbol{u} = u_B(r,\varphi,t)\ \boldsymbol{e}_B + \alpha(r)\boldsymbol{\nabla}\psi(r,\varphi,t) \times \boldsymbol{e}_B \qquad (4)$$

where $u_B(r,\varphi,t)$ is the velocity component along $\boldsymbol{e}_B(r,\theta)$ and $\psi(r,\varphi,t)$ is a streamfunction. Note that the vorticity field can be expressed as follows :

$$\boldsymbol{\omega} = \omega_B(r,\varphi,t)\ \boldsymbol{e}_B + \alpha\boldsymbol{\nabla}\left(\frac{u_B(r,\varphi,t)}{\alpha}\right) \times \boldsymbol{e}_B\,. \qquad (5)$$

The vorticity component along $\boldsymbol{e}_B$ is linked to the streamfunction ψ *as well as* to u_B by the following relationship

$$\omega_B = -\mathbb{L}\psi + \frac{2\alpha^2}{L}u_B \qquad (6)$$

where the linear operator $\mathbb{L}$ stands for

$$\mathbb{L}(\cdot) = \frac{1}{r\alpha}\frac{\partial}{\partial r}\left(r\alpha^2\frac{\partial}{\partial r}(\cdot)\right) + \frac{1}{r^2\alpha}\frac{\partial^2}{\partial\varphi^2}(\cdot)\,. \qquad (7)$$

The total vorticity and velocity fields are thus given by only two scalar fields $\omega_B(r,\varphi,t)$ and $u_B(r,\varphi,t)$. The streamfunction $\psi(r,\varphi,t)$ is slaved to these variables through equation (6).
In order to describe the flow evolution, we hence have to obtain two dynamical equations for quantities $\omega_B(r,\varphi,t)$ and $u_B(r,\varphi,t)$. This formulation is a generalization of the standard 2D ψ–ω method.

Indeed the 3D Navier–Stokes problem for a helical symmetric flow can be reduced to a dynamical equation for $u_B(r,\varphi,t)$ and $\omega_B(r,\varphi,t)$. The first equation reads as

$$\partial_t u_B + NL_u = VT_u \tag{8}$$

where the nonlinear and viscous terms are given by

$$\begin{aligned} NL_u &\equiv \boldsymbol{e}_B \cdot [\boldsymbol{\omega} \times \boldsymbol{u}]\,, \\ VT_u &\equiv \nu \left[\mathbb{L}(\frac{u_B}{\alpha}) - \frac{2\alpha^2}{L}\omega_B \right]. \end{aligned} \tag{9}$$

The dynamical equation for ω_B reads

$$\partial_t \omega_B + NL_\omega = VT_\omega \tag{10}$$

where the nonlinear is given by

$$NL_\omega \equiv \boldsymbol{e}_B \cdot \boldsymbol{\nabla} \times [\boldsymbol{\omega} \times \boldsymbol{u}]\,, \tag{11}$$

and the viscous term by

$$\begin{aligned} VT_\omega &\equiv -\nu\, \boldsymbol{e}_B \cdot \boldsymbol{\nabla} \times [\boldsymbol{\nabla} \times \boldsymbol{\omega}] \\ &= \nu \left[\mathbb{L}(\frac{\omega_B}{\alpha}) - \left(\frac{2\alpha^2}{L}\right)^2 \omega_B \right. \\ &\qquad \left. + \frac{2\alpha^2}{L}\mathbb{L}(\frac{u_B}{\alpha}) \right]. \end{aligned} \tag{12}$$

3 Numerical formulation

As variable $\varphi = \theta - z/L$ is 2π-periodic, the fields can be expressed as Fourier series along that direction. We hence introduce the "azimuthal" modes $u_B^{(m)}(r,t)$, $\omega_B^{(m)}(r,t)$ and write equations (8) and (10) for each Fourier mode m (m is a positive integer). For the axisymmetric mode $m = 0$, the dynamical equations are written for the real Fourier modes $u_B^{(0)}(r,t)$ and $u_\varphi^{(0)}(r,t)$, instead of $\omega_B^{(0)}(r,t)$. From quantities $u_B^{(m)}(r,t)$, $\omega_B^{(m)}(r,t)$ for $m \neq 0$, one obtains the values $\psi^{(m)}(r,t)$ for $m \neq 0$ using equation (6) written for mode m :

$$\mathbb{L}^{(m)}\psi^{(m)} = -\omega_B^{(m)} + \frac{2\alpha^2}{L}u_B^{(m)} \tag{13}$$

where the operator $\mathbb{L}^{(m)}$ is given by

$$\mathbb{L}^{(m)}(\cdot) = \frac{1}{r\alpha}\frac{\partial}{\partial r}\left(r\alpha^2\frac{\partial}{\partial r}(\cdot)\right) - \frac{m^2}{r^2\alpha}(\cdot)\,, \tag{14}$$

together with the boundary conditions for $\psi^{(m)}(r,t)$. The time evolution of mode $u_B^{(m)}(r,t)$ is governed by

$$\partial_t u_B^{(m)} + NL_u^{(m)} = VT_u^{(m)}\,. \tag{15}$$

As the viscous term VT_u is a linear term, one directly obtains

$$VT_u^{(m)} = \nu\left[\mathbb{L}^{(m)}(\frac{u_B^{(m)}}{\alpha}) - \frac{2\alpha^2}{L}\omega_B^{(m)}\right]. \tag{16}$$

There is no such simple expression for nonlinear terms : NL_u has to be first evaluated in the physical space and is then Fourier-transformed to yield $NL_u^{(m)}$. The time evolution for modes $\omega_B^{(m)}(r,t)$ with $m \neq 0$ and mode $u_\varphi^{(0)}(r,t)$ is treated in a similar way. The code has been adapted from a pure 2D code written by O. Daube [8]. The time advance of any of these modes is performed using second order backward discretisation of the temporal derivative. Nonlinear terms appear explicitly through second order Adams–Bashforth extrapolation whereas the viscous term has been made implicit.

Boundary conditions should be also imposed for ${\omega_B}^{(m)}$ with $m \neq 0$, ${u_B}^{(m)}$ and ${u_\varphi}^{(0)}$. In addition to regularity conditions at $r = 0$, one should impose conditions at the outer boundary taken to be at $r = R_{\text{ext}}$:

$$\begin{aligned} &{\omega_B}^{(m)}(R_{\text{ext}}) = 0, \quad {u_B}^{(m)}(R_{\text{ext}}) = 0 \;\text{ for }\; m \neq 0, \\ &u_B^{(0)}(R_{\text{ext}}) = \alpha(R_{\text{ext}})\left(U_z^\infty + \frac{\Gamma}{2\,\pi\,L}\right). \end{aligned} \tag{17}$$

A boundary condition for ${u_\varphi}^{(0)}$ is also imposed at the outer boundary. These conditions are described in a much more detailed way in [9].

For spatial discretization, two series of N_r grid points are defined in the radial direction :

$$\left| \begin{array}{l} r_i = (i-1)\delta r \\ r_i^+ = r_{i+\frac{1}{2}} = r_i + \delta r/2 \end{array} \right. \qquad (i = 1, \cdots, N_r)\,,$$

where $\delta r = R_{\text{ext}}/(N_r - 1)$ and only one set of N_θ grid points in the azimuthal direction :

$$\varphi_j = j\,\delta\varphi \quad (j = 0, \cdots, N_\theta - 1), \quad \varphi_{N_\theta} = \varphi_0 = 0\,,$$

where $\delta\varphi = 2\pi/N_\theta$. In physical space, quantities $u_B(r,\varphi,t)$, $\omega_B(r,\varphi,t)$, $\psi(r,\varphi,t)$, radial components $u_r(r,\varphi,t)$ and $\omega_r(r,\varphi,t)$ are defined at points (i,j) (which stands thereafter for (r_i,φ_j)). Azimuthal components $u_\varphi(r,\varphi,t)$ and $\omega_\varphi(r,\varphi,t)$ live at points $(i+\frac{1}{2},j)$.

Nonlinear terms such as $NL_u^{(m)}$ are needed at points r_i, so that we have to compute the nonlinear terms $NL_u = (\boldsymbol{\omega} \times \boldsymbol{u})_B = \omega_r\, u_\varphi - \omega_\varphi\, u_r$ in physical space at points (i,j). To summarize, one needs to

evaluate various quantities at different grid points : $\omega_r\, u_\varphi$, $\omega_\varphi\, u_r$ at points (i,j), $\omega_B\, u_r$ at points $(i+\frac{1}{2},j)$, $-\omega_B\, u_\varphi$ at points (i,j) and u_B^2 at points (i,j).
The resolution of the dynamical equations requires the radial discretization of operators $\mathbb{L}^{(m)}$, $VT_u^{(m)}$,$VT_\omega^{(m)}$ at each radial location r_i with $2 \le i \le N_r - 1$. This is performed with a second order centered scheme : according to the dynamical equation considered, the resulting system has a tridiagonal, pentadiagonal or hexadiagonal structure, and is solved using a band LU factorization of the LAPACK library. As each mode m is treated independently, parallel computing with shared memory can be most conveniently implemented.

4 Quasi-steady helical vortices

Here we simulate the evolution of a single helical vortex with small core size at a low value of the reduced pitch $L = 0.5$. The initial profile is given by

$$\omega_B = \frac{\Gamma_0}{\pi a_0^2} \exp[-(\boldsymbol{r}-\boldsymbol{r}_0)^2/a_0^2]\,, \tag{18}$$

$$\text{and} \quad \frac{u_B}{\alpha} = \frac{\Gamma_0}{2\,\pi\, L}\,, \tag{19}$$

with $\Gamma_0 = \pi$, $\boldsymbol{r}_0 = (1,0)$, $a_0 = 0.1$. The Reynolds number is set to $Re = \Gamma_0/\nu = 1000$. The numerical simulation is performed with a domain of radial extent $R_{\text{ext}} = 2$ meshed by 512×256 grid points.

The temporal evolution of the helical vorticity component ω_B is shown on figure 3. At short times, small helical filaments are rapidely formed ($t = 0.08, 0.012$) and destroyed ($t = 0.2, 0.4$). Thereafter the vortex adopts a shape that remains nearly constant. For $t > 0.4$, it evolves on a slow time scale imposed by viscous diffusion and proportional to the Reynolds number. The helical vortex has thus reached a quasi-steady state when considered in a reference frame rotating with it at frequency ω.

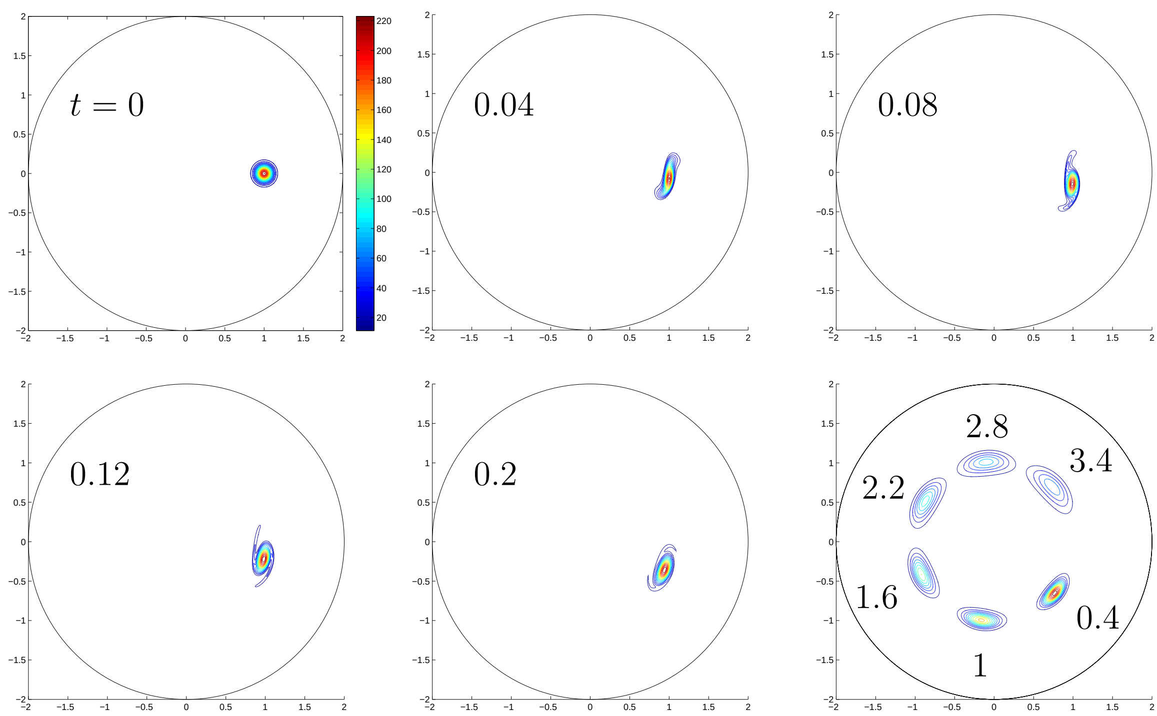

FIGURE 3 – *Convergence of a single helical vortex towards a quasi-steady state : temporal evolution of the helical vorticity component ω_B at $Re = 1000$. The helix pitch is set to $L = 0.5$ and the initial helical vortex is such that* $\Gamma_0 = \pi$, $r_0 = ||\boldsymbol{r}_0|| = 1$, $a_0 = 0.1$

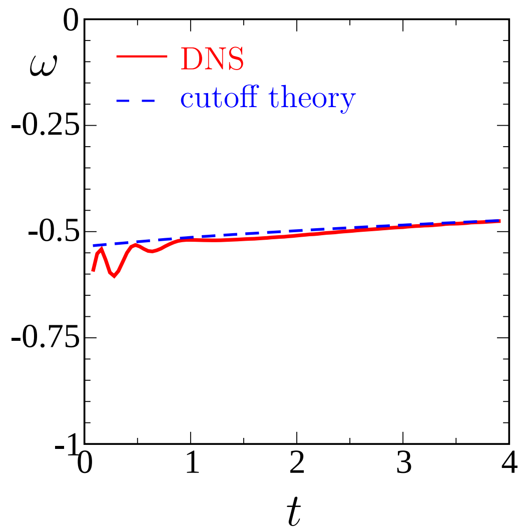

FIGURE 4 – *Angular velocity $\omega(t)$ of the helical vortex of figure 3. Comparaison between DNS and semi-analytical cutoff theory.*

Measuring the angular velocity $\omega(t)$ obtained by DNS and comparing with the theoretical value obtained by the cutoff theory is one of the validation tests of the numerical code. The cutoff results are here semi-analytical since they use the quantities core size $a(t)$, distance $r_{\max}(t)$ from the axis and core circulation $\Gamma(t)$ evolving in time and given by the DNS. The comparison is shown in figure 4, and is found very satisfactory once the filaments have been destroyed and that the vortex has reached its quasi-steady state.

It should be noted that vorticity isocontours in figure 3 are presented in a plane perpendicular to the z-axis : the curved/elongated shape adopted by the vortex for $t \geq 0.4$ corresponds in fact to a quasi-circular core shape when considered in an inclined plane perpendicular to the vortex tube.

This can also be seen on figure 5, presenting a quasi-steady state made of two helical vortices. In this snapshot, the 3D helical structure of the vortex has been materialised. It is clearly seen that the cores are indeed close to circular while they are strongly deformed in the bottom plane perpendicular to z.

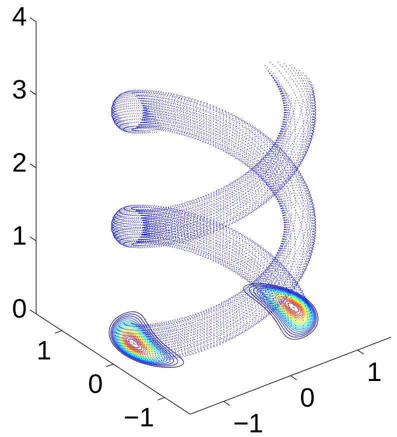

FIGURE 5 – *Quasi-steady state for two vortices represented in 3D. $L = 0.5$.*

The numerical code thus makes it possible to obtain quasi-steady states of the Navier–Stokes equations with one or several helical vortices of given pitch. Note that the three-dimensional stability of these obtained solutions is not known since helical symmetry is enforced by the current formulation. Some states are stable, but other might be unstable with respect to perturbations breaking the helical symmetry. In this latter case however, the present numerical code is able to generate unstable basic helical flows that can be injected for instance in a fully three-dimensional code in order to determine various instability properties. This corresponds to future work.

5 Helical vortex merging

The above helical quasi-steady states evolve, as already mentionned, on a slow time scale associated to viscous diffusion. In the pure two-dimensional case ($L = \infty$), it is known that two identical vortices rotate around each other for a period of time proportional to Reynolds number [10]. Eventually, their mutual distance suddenly decreases and after some rapid oscillations vanishes, indicating that the vortices have merged. The distance of a maximum of vorticity from the z-axis during this process is plotted in figure 6 (leftmost curve). Note that it is made nondimensional using the initial separation distance between the two maxima of vorticity so that $r_{\max}(0) = r_0 = 0.5$.

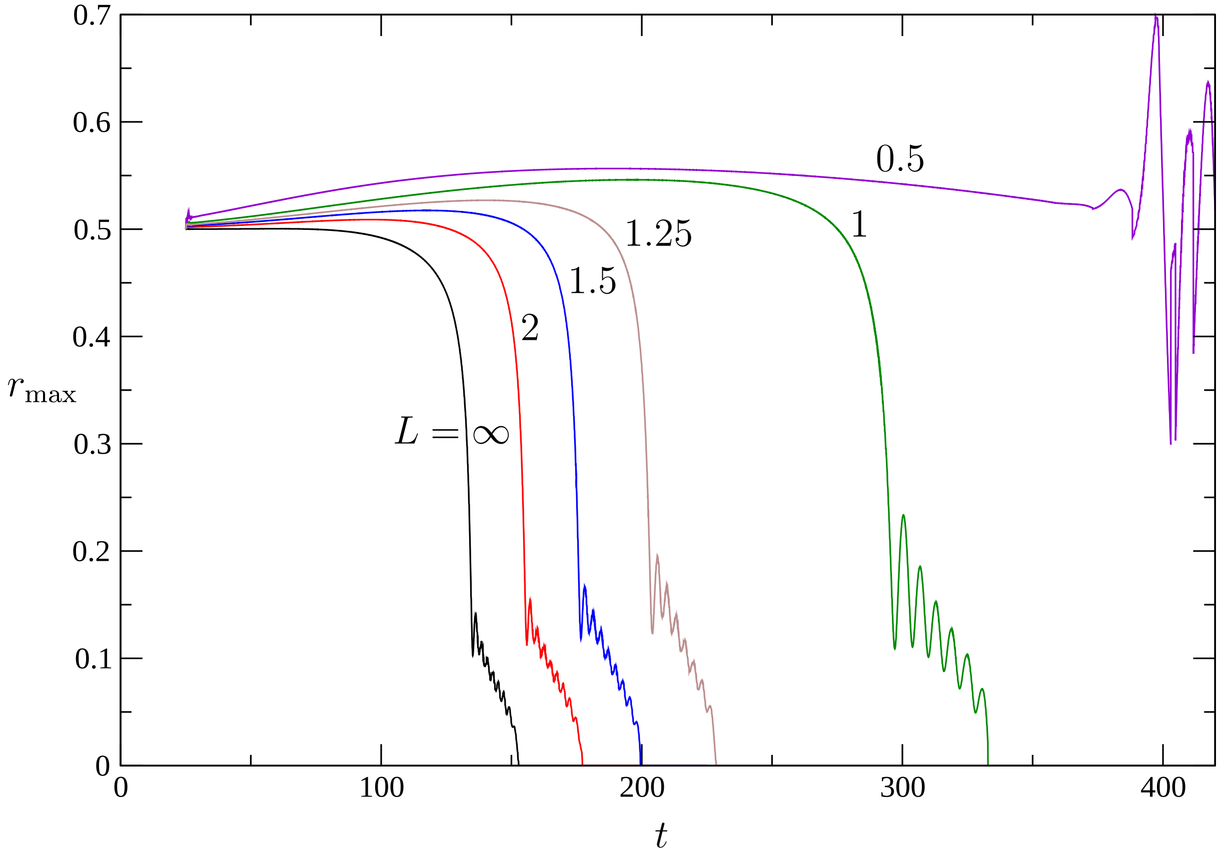

FIGURE 6 – *Merging of two helical vortices at $Re = 10000$ for different values of L. Time evolution of the distance $r_{\max}$ of one of the vortices from the axis. Initial helices $\Gamma_0 = 1$, $r_0 = 0.5$, $a_0 = 0.1$.*

Numerical simulations have been performed at the same Reynolds number $Re = 10000$ but for helical vortices at finite L values. The figure 6 shows that decreasing L progressively slows down the process, since at $L = 1$ the merging time has roughly doubled with respect to the 2D case $L = \infty$.

Figure 6 reveals another phenomenon : as L is further decreased (on the figure for $L = 0.5$) the curve $r_{\max}(t)$ drastically changes. Near time $t = 380$, its behaviour becomes strongly erratic. Figures 7 and 8 show the time evolution of the helical component ω_B of vorticity for $L = 1$ and $L = 0.5$ respectively. The case $L = 1$ resembles the pure 2D case $L = \infty$, however with the major difference that the vortex after merging is found to be strongly elliptical ($t = 325$) and seems to remain so for a long time : at $t = 425$, for instance, it still has got almost the same shape (since it is centered on the z-axis, this is no oblique cut artefact). Beside the helical symmetry, the two-vortex initial condition is invariant through the transformation $\varphi \to \varphi + \pi$. For the largest investigated values of the reduced pitch ($L \geq 1$), this additional symmetry is preserved during the whole simulation. By contrast, the dynamics for $L \leq 0.5$ plotted in figure 8 shows that it can break at some time : one of the two helical vortices comes “inside” the other (see $t = 385$) and thereafter their interaction becomes complex. Symmetry breaking causes the periodicity along the azimuthal direction θ to change from its initial value π to the value 2π, and therefore the periodicity along the axial direction z also changes from πL to $2\pi L$. The phenomenon has much in common with the subharmonic pairing instability of a row of straight vortices or of vortex rings. The merging process at low $L \leq 0.5$ involves two neighbouring spires and is very similar to the merging of two vortex rings [11] while at higher $L \geq 1$ it involves facing helical vortices. As a consequence, the merged structure is a screwdriver type of helical vortex at low L (not shown), while at higher L, it is a twisted elliptical vortex centered at the origin (see figure 7 at $t = 425$).

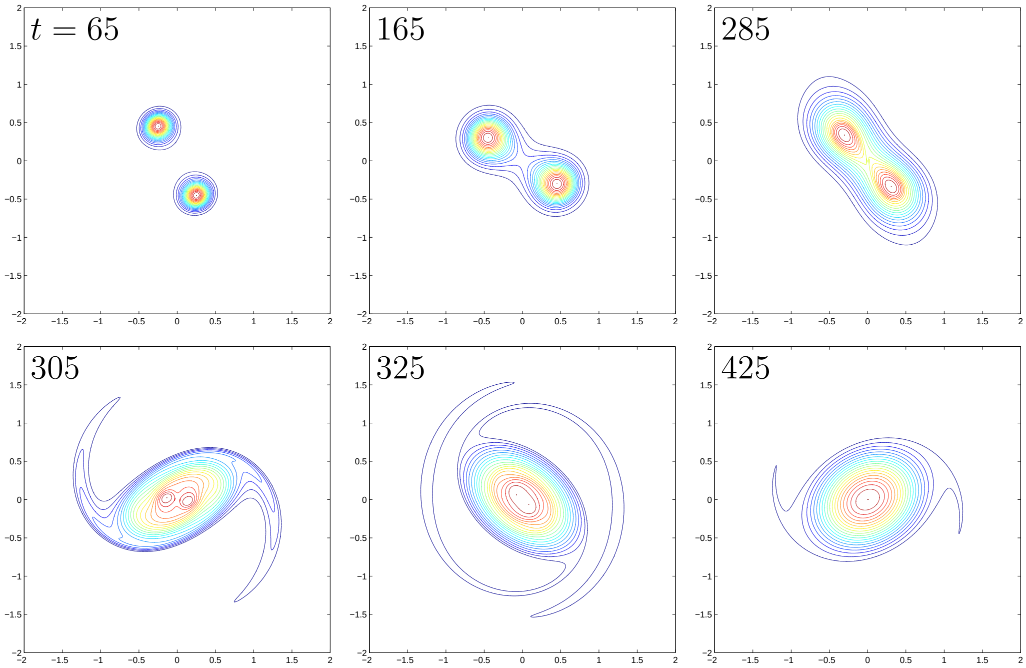

FIGURE 7 – *Snapshots of the helical vorticity component* ω_B *during the merging of two helical vortices with* $L = 1$ *at* $Re = 10000$. *Initial helices are such that* $\Gamma_0 = 1$, $r_0 = 0.5$, $a_0 = 0.1$.

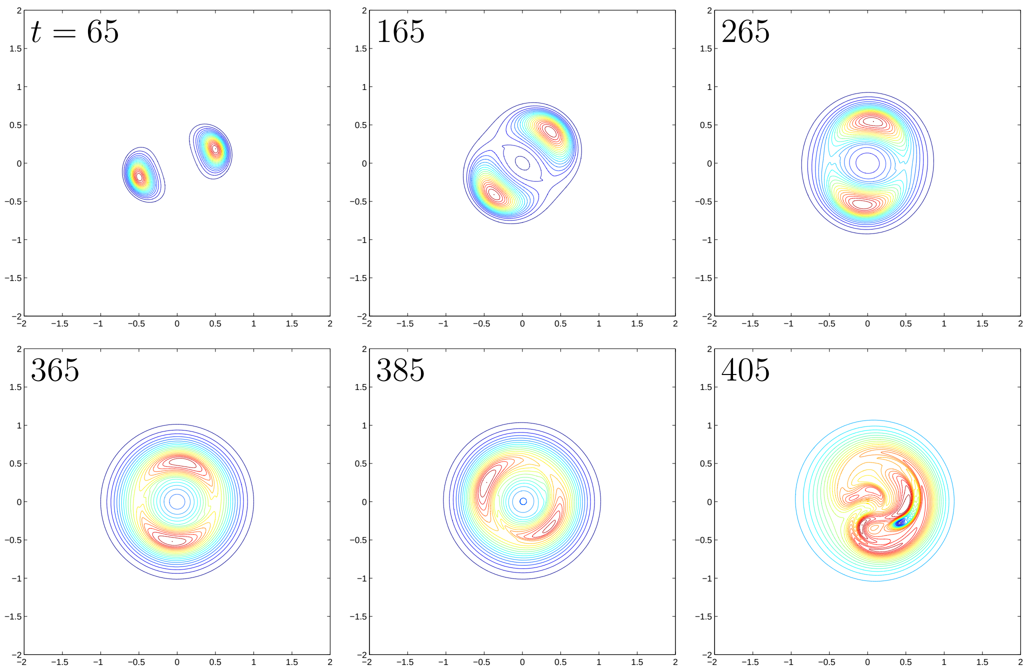

FIGURE 8 – *Snapshots of the helical vorticity component* ω_B *during the merging of two helical vortices with* $L = 0.5$ *at* $Re = 10000$. *Initial helices are such that* $\Gamma_0 = 1$, $r_0 = 0.5$, $a_0 = 0.1$.

6 Concluding remarks

In this paper, we present an original DNS code aimed at solving the Navier–Stokes equations for incompressible flow with helical symmetry. In this framework, the dynamics is governed by a set of three coupled equations for the helical components of vorticity ω_B, of velocity u_B and for the helical streamfunction ψ. The code is shown to give access to quasi-equilibrium states representing one or several helical vortices. The present code has several advantages : while taking into account three-dimensional effects of curvature and torsion, the resolution is basically of the 2D type, which allows for finer grids, higher Reynolds numbers and longer integration times. For example, this allows one to investigate the long-time dynamics of merging of two indentical helical vortices at $Re = 10000$. It has been found that, at high and moderate values of the helix pitch, the merging process is similar to the one obtained in pure 2D dynamics. By contrast, for smaller values of the pitch, merging also occurs but in a quite different fashion : adjacent spires interact two by two as in a subharmonic instability process while remaining helically symmetrical. Of course, this latter symmetry may not hold in a three-dimensional framework, and some results of the present study should be confronted to fully 3D computations.

References

[1] B. G. Green, E. A. Gillies, and R. E. Brown The flow field around a rotor in axial descent. *J. Fluid Mech.* **534**, 237–261.

[2] J. C. Hardin (1982) The velocity field induced by a helical vortex filament. *Phys. Fluids* **25**(11), 1949–1952.

[3] S. E. Widnall (1972) The stability of a helical vortex filament. *J. Fluid Mech.* **54**, 641–663.

[4] D. W. Moore, and P. G. Saffman (1972) The motion of a vortex filament with axial flow. *Philos. Trans. R. Soc. London, Ser. A* **272**, 403–429.

[5] P. A. Kuibin, and V. L. Okulov (1998) Self-induced motion and asymptotic expansion of the velocity field in the vicinity of a helical vortex filament. *Phys. Fluids* **10**, 607–614.

[6] Y. Fukumoto, and V. L. Okulov (2005) The velocity field induced by a helical vortex tube. *Phys. Fluids* **17**, 107101.

[7] D. Lucas, and D. G. Dritschel (2009) A family of helically symmetric vortex equilibria. *J. Fluid Mech.* **634**, 245–268.

[8] O. Daube (1992). Resolution of the 2D Navier–Stokes equations in velocity/vorticity form by means of an influence matrix technique. *J. Comp. Phys.* **103**, 402–414.

[9] I. Delbende, and M. Rossi (2010) DNS of flows with helical symmetry. *To be published.*

[10] C. Josserand, and M. Rossi (2007) The merging of two co-rotating vortices : a numerical study. *Eur. J. Mech. B/Fluid.* **26**, 779–794.

[11] N. Riley, and D. P. Stevens (1992) A note on leapfrogging vortex rings. *Fluid Dyn. Res.* **11**, 235–244.